Embedded silver PDMS electrodes for single cell electrical impedance spectroscopy

2016 J. Micromech. Microeng. 26 095006

(http://iopscience.iop.org/0960-1317/26/9/095006)

IOP Publishing Journal of Micromechanics and Microengineering
J. Micromech. Microeng. **26** (2016) 095006 (10pp) doi:10.1088/0960-1317/26/9/095006

Embedded silver PDMS electrodes for single cell electrical impedance spectroscopy

Yuan Wei[1,6], Zhensong Xu[1,6], Mark A Cachia[1], John Nguyen[1], Yi Zheng[1,2], Chen Wang[4,5] and Yu Sun[1,2,3,7]

[1] Department of Mechanical & Industrial Engineering, University of Toronto, Toronto, ON, Canada
[2] Institute of Biomaterials & Biomedical Engineering, University of Toronto, Toronto, ON, Canada
[3] Department of Electrical & Computer Engineering, University of Toronto, Toronto, ON, Canada
[4] Department of Pathology & Laboratory Medicine, Mount Sinai Hospital, Toronto, ON, Canada
[5] Department of Laboratory Medicine & Pathobiology, University of Toronto, Toronto, ON, Canada

E-mail: sun@mie.utoronto.ca

Received 3 March 2016, revised 5 June 2016
Accepted for publication 21 June 2016
Published 6 July 2016

Abstract

This paper presents a microfluidic device with wide channels and embedded AgPDMS electrodes for measuring the electrical properties of single cells. The work demonstrates the feasibility of using a large channel design and embedded electrodes for impedance spectroscopy to circumvent issues such as channel clogging and limited device re-usability. AgPDMS electrodes were formed on channel sidewalls for impedance detection and cell electrical properties measurement. Equivalent circuit models were used to interpret multi-frequency impedance data to quantify each cell's cytoplasm conductivity and specific membrane capacitance. T24 cells were tested to validate the microfluidic system and modeling results. Comparisons were then made by measuring two leukemia cell lines (AML-2 and HL-60) which were found to have different cytoplasm conductivity values (0.29 ± 0.15 S m^{-1} versus 0.47 ± 0.20 S m^{-1}) and specific membrane capacitance values (41 ± 25 mF m^{-2} versus 55 ± 26 mF m^{-2}) when the cells were flown through the wide channel and measured by the AgPDMS electrodes.

Keywords: silver PDMS, impedance spectroscopy, microfluidics, composite electrodes, electrical measurement

(Some figures may appear in colour only in the online journal)

1. Introduction

Polydimethylsiloxane (PDMS) has been a mainstream material for constructing microfluidic devices due to its favourable physical and chemical properties, such as flexibility, nontoxicity, biocompatibility, chemical inertness, gas permeability, and ease of fabrication [1]. PDMS-based devices are simpler to build and less costly than silicon or glass-based devices, allowing for rapid prototyping and design iterations. Therefore, there has been interest in developing PDMS-based conducting composite electrodes for integration into PDMS microfluidic devices to maintain straightforward fabrication and realize electrical measurement of conductivity and membrane capacitance. These composites should have similar mechanical properties of PDMS while still being appropriately conductive for their relevant applications. Note that PDMS composites can be simply fabricated via screen printing or photopatterning, compared to more intensive methods for forming metal electrodes (e.g. via sputtering or evaporation) [2–6].

[6] These authors contributed equally to this work.
[7] Department of Mechanical & Industrial Engineering, University of Toronto, 5 King's College Road, Toronto, ON M5S 3G8, Canada.

In conductive PDMS composites, percolation theory states that there is a threshold of conductive particle concentration at which a continuous chain is formed, resulting in macroscopic conductivity [7]. This threshold depends on several factors, including the size of the conductive particles, the geometry of the particles, and the mixing procedure. Increasing the conductive particle concentration beyond this threshold leads to a significant decrease in resistivity. Thus, given a sufficient concentration of the conductive filler particles, the composite can be rendered highly conductive. For instance, silver (Ag) coated copper (Cu) flakes were mixed with PDMS to achieve conductivities greater than 10^4 S m^{-1} at concentrations between 75 wt% and 85 wt% [8]. Carbon PDMS (CPDMS) composites were found to be conductive above 10 wt% although the conductivity was much lower (on the order of 10 S m^{-1}) [4, 9]. CPDMS has been tested in several applications including microfluidic valves [10], pumps [11], and mixers [12].

Silver has been of particular interest in PDMS composite electrodes due to its desirable wetting properties [5] and suitability for biological applications [13]. Ag yields the lowest interfacial impedance, compared to other metals such as titanium and copper, which is important for minimizing signal distortion [14]. Ferromagnetic metals such as nickel have been shown to induce a magnetic field that can affect electrical measurements [15, 16] while silver does not cause such complications. Silver PDMS (AgPDMS) is also much more conductive than CPDMS, reaching conductivities greater than 10^4 S m^{-1} [4]. AgPDMS electrodes have previously been used in several applications. For instance, AgPDMS was used in temperature-dependent devices, such as a microheater and thermochromics display [5, 17, 18]. AgPDMS conductivity also varies as a function of strain, showing potential as a pressure sensor [4, 6]. Finally, AgPDMS has been used in droplet detection applications, where impedance signals reflects droplet size [19]. Despite these applications, AgPDMS electrodes have not yet been investigated for performing impedance spectroscopy.

Impedance spectroscopy is a useful technique for measuring the electrical properties of cells, including size and size-independent quantities such as cytoplasm conductivity and specific membrane capacitance [20, 21]. In this technique, the cell is typically modeled as a single-shelled sphere. The cell membrane is represented as a thin dielectric shell, which contains the homogeneous resistive cytoplasm. The first electrical measurement technique on single cells was the Coulter counter which measures direct current (DC) impedance signals for counting and sizing single cells [22]. It was later discovered that using a high frequency signal simultaneous to a low frequency signal can detect both resistive and capacitive changes caused by cells [23]. Different cells have different ion concentrations and nucleus-to-cytoplasm volume ratios as well as different protein expressions and lipid bilayer compositions. These factors affect the cytoplasm conductivity and specific membrane capacitance of a cell, respectively [24, 25].

Several microfluidic designs have been developed that use multiple frequencies to electrically probe single cells as they pass through a small channel (in the range of the cell size) where the electric field lines are concentrated [26–31]. Early devices used integrated gold (Au) electrodes situated on microchannel sidewalls for detecting impedance differences in blood cells [26]. Co-planar and parallel platinum (Pt) electrodes were also used for cell analysis and sizing [27, 29]. It was demonstrated that the parallel electrode configuration generated a more uniform electric field and was therefore less susceptible to the position of particles compared to the co-planar configuration [32]. The parallel configuration also had greater sensitivity due to the more confined electric field compared to the co-planar configuration. Two sets of embedded Pt electrodes, one for sensing and one for reference, provided more accurate differential measurements of cell impedance, and were used to differentiate leukocyte sub-populations [30, 31, 33]. The embedded electrode design has been used to probe single cells at high frequencies (>1 MHz), which is necessary for measuring intracellular characteristics [20]. Plug-in Ag/AgCl electrodes were used to minimize the electrical double-layer (EDL) effect [28]. The device had a constriction channel that was smaller than the cell, allowing for lower frequency measurements and more accurate cell sizing. Measurement was limited to sub-MHz frequencies due to stray capacitance effects [28]. Although these existing devices used different electrode configurations, their detection microchannels were all designed to be close to the size of the cell for sensitivity requirements. However, these small channels (often <20 μm) are subject to practical issues, such as clogging of the device due to contaminants and cell debris. Additionally, using AgPDMS permits easy formation of thick electrodes in a parallel configuration which ensures a more uniform electric field (versus planar electrodes). Thus, this work aimed to investigate the feasibility of using larger channels and embedded composite electrodes to measure the electrical properties of single cells.

Properly choosing the electrode material is important for reducing or avoiding the EDL effect. Solid metal electrodes have been shown to exhibit a high EDL (with capacitance on the order of 0.1 F m^{-2}) [34], caused by the interaction at the interface of the metal electrodes and the ionic solution, which can significantly affect low frequency impedance data [26]. Embedded Ag/AgCl electrodes were previously reported [35]. Although these electrodes are effective in mitigating the EDL effect, the planar Ag/AgCl electrodes and their configuration did not generate a uniform electric field as desired for impedance spectroscopy. In addition, the fabrication of microfluidic devices integrated with metal or metal chloride electrodes has a complex fabrication process as the alignment and bonding of separate pieces are required, as opposed to a single solid structure [2, 35]. Hence, there have been efforts to develop polymer-based conducting composite electrodes.

This paper reports a wide channel, AgPDMS embedded electrode microfluidic device that is capable of measuring cytoplasm conductivity and specific membrane capacitance of single cells. The large channel design overcomes device clogging and permits multi-use of the devices. AgPDMS composite was fabricated and used to form sidewall electrodes for impedance measurement. Experimental results demonstrate that the device has adequate sensitivity for the electrical measurement of cells. Multi-frequency impedance data was fitted to equivalent circuit models to quantify cytoplasm conductivity and specific membrane capacitance of each cell. T24 human

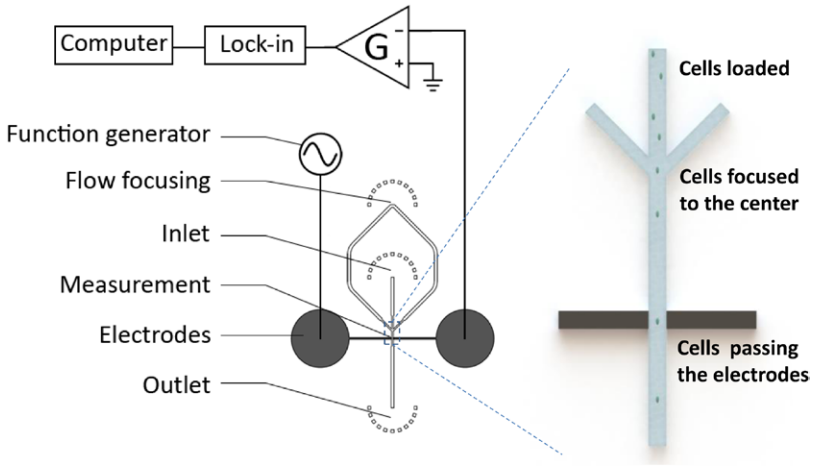

Figure 1. Schematic diagram of the microfluidic device for single cell impedance measurement. AgPDMS electrodes are embedded on the sidewalls of the microchannel. Impedance at eight frequencies is measured as a cell flows through the measurement region.

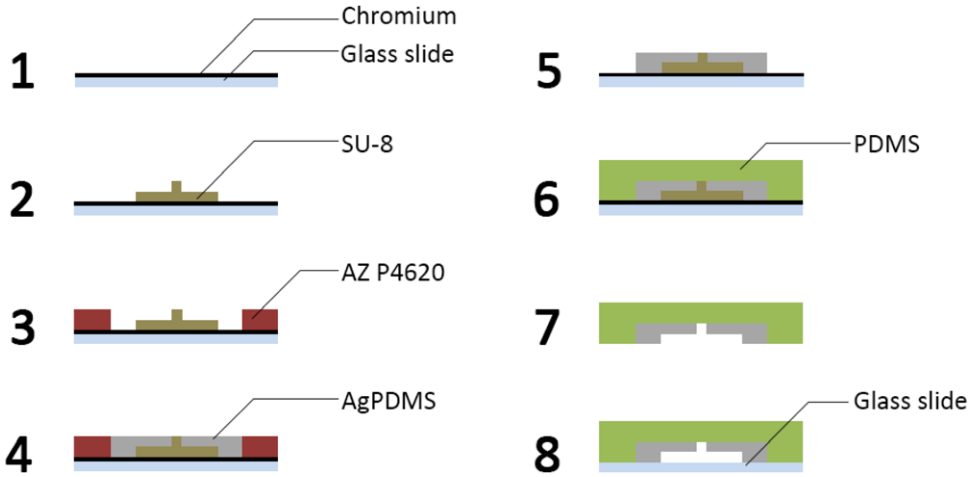

Figure 2. Process flow of device fabrication and AgPDMS electrode formation. 1. A chromium layer was first patterned on a glass slide. 2. SU-8 was used to create a master. 3. AZ P4620 was patterned to create a sacrificial mold for the AgPDMS electrodes. 4. The AgPDMS composite was then spread into the mold and cured. 5. The AZ P4620 layer was dissolved. 6. PDMS was poured onto the mold and cured. 7. The entire PDMS and AgPDMS structure was peeled off. 8. The entire structure was bonded to a clean glass slide.

bladder cancer cells were measured to verify the feasibility of the wide channel design for data collection. AML-2 and HL-60 leukemia cells were tested to validate the device and the models. These two leukemia cell lines were determined to have different values in cytoplasm conductivities (0.29 ± 0.15 S m^{-1} and 0.47 ± 0.20 S m^{-1}) and specific membrane capacitances of (41 ± 25 mF m^{-2} and 55 ± 26 mF m^{-2}).

2. System overview

Figure 1 shows a schematic diagram of the single cell impedance measurement system. The microfluidic device is made of PDMS, with parallel 3D AgPDMS electrodes embedded on the sidewalls of a 100 μm wide microchannel. A function generator is used to generate a sinusoidal excitation input voltage at eight different frequencies (11 kHz, 101 kHz, 401 kHz, 701 kHz, 1.01 MHz, 2.01 MHz, 4.01 MHz, 6.01 MHz) at 0.4 V_{p-p}. This voltage was selected to optimize the SNR without risking the electroporation of cells (40 V cm^{-1} in this work versus >200 V cm^{-1} as required for electroporation [36]). Current in the microchannel is pre-amplified and demodulated at a sampling rate of 14.4 kHz for each frequency component. Cells are loaded in the inlet and are pressure driven at 100 Pa to travel to the outlet. Flow focusing branches are used to position cells to the center of the microchannel as cells pass by the measurement region to minimize impedance distortion. When a cell passes through the microchannel, the impedance at each of the eight frequencies is measured. The impedance profile is fitted to equivalent circuit models to determine cytoplasm conductivity and specific membrane capacitance of the cell.

3. Materials and methods

3.1. Electrode and device fabrication

The microfluidic chip was fabricated using standard photolithography and a modified screen printing process [4, 19, 37]. The process flow is summarized in figure 2. A chromium layer was first patterned on a glass slide for the alignment of multiple layers (figure 2(1)). SU-8 2000 (MicroChem, Newton,

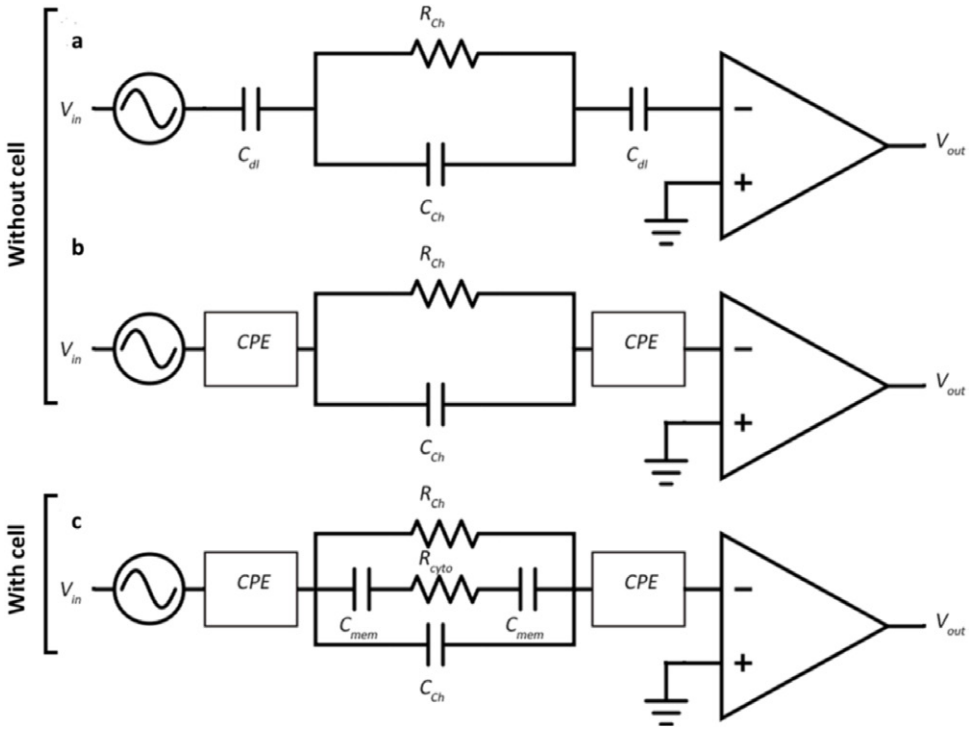

Figure 3. (a) The device without a cell in the microchannel. Double layer is modeled as an ideal capacitor. (b) Without a cell, the double layer effect is modeled as a CPE. (c) Device with a cell, which is modeled as two capacitors (representing the membrane capacitance) in series with a resistor (representing the cytoplasm resistance).

MA, USA) was used to create a master having a height of 50 μm (figure 2(2)) measured by profilerometry. AZ P4620 (Capitol Scientific, Austin, TX, USA) was then spin-coated and patterned to create a sacrificial mold (50 μm in height) for the AgPDMS electrodes (figure 2(3)). Ag particles of 2–3.5 μm in size (Sigma-Aldrich, St. Louis, MO, USA) were mixed with PDMS (Ellsworth Adhesives, Stoney Creek, ON, Canada) using a mortar and pestle. The AgPDMS composite was then spread into the mold, with excess AgPDMS removed using a razor blade to obtain the desired pattern. The master was baked at 70 °C for 30 min to cure the AgPDMS, and then washed in acetone to dissolve the AZ P4620 layer, followed by methanol and DI water rinsing (figure 2(4)). PDMS was then poured onto the mold and cured on the hotplate at 150 °C for 10 min. The entire PDMS and AgPDMS structure was peeled off the SU-8 master (figures 2(5)–(7)). AgPDMS was found to bond strongly to PDMS, which was then O_2 plasma bonded to a clean glass slide (figure 2(8)). The final microchannel is 100 μm wide and 50 μm high, and the AgPDMS electrodes have a length of 100 μm along the sidewall and a height of 50 μm.

3.2. Cell preparation

T24 (bladder carcinoma), AML-2 (acute myeloid leukemia), and HL-60 (human promyelocytic leukemia) cell lines were used in this work due to the availability of previous literature data on these cell types [28, 38, 39]. T24 cells were purchased from the American Type Culture Collection (ATCC, Manassas, VA, USA) and were cultured in ATCC-formulated McCoy's 5a modified medium supplemented with 10% fetal bovine serum (FBS) (Life Technologies, Grand Island, NY, USA) and 1% penicillin (Life Technologies, Grand Island, NY, USA). AML-2 and HL-60 were obtained from Mount Sinai Hospital (Toronto, ON, Canada) and were cultured in Dulbecco's Modified Eagle's Medium (Sigma-Aldrich, St. Louis, MO, USA) supplemented with 10% FBS and 1% penicillin.

All cell lines were incubated at 37 °C with 100% humidity and 5% CO_2. Prior to experiments, cells were centrifuged and re-suspended in phophaste-buffered saline (PBS) (Life Technologies, Grand Island, NY, USA)with 1% w/v bovine serum albumin (BSA) (Life Technologies, Grand Island, NY, USA). The microfluidic device was also loaded with PBS with 1% w/v BSA to reduce cell adhesion on channel walls [28, 40, 41]. For testing the reusability of the device, de-ionized (DI) water was used to flush through the device at the end of each experiment for cleaning purposes. One device was used for all of the experiments reported here.

3.3. Equivalent circuit models

Electric properties of a single particle positioned between two parallel electrodes can be modeled with Maxwell's mixture theory [30, 42, 43]. Given the geometrical parameters of our microfluidic system (i.e. electrode and channel dimensions), the system with and without the presence of a cell is represented by two equivalent circuit models. The microchannel filled with PBS is represented by an equivalent resistance R_{Ch} and capacitance C_{Ch}.

The AgPDMS electrodes induce an electrical double layer (EDL) due to the ionic nature of the PBS solution. In the parallel-plate electrode configuration, the EDL can be modeled as an ideal capacitor C_{dl}, as shown in figure 3(a). However, if the electrode is not perfectly polarizable due to inhomogeneities

on the electrode surface, the EDL may be better represented as a constant phase element (CPE), which has both resistive and capacitive qualities [44, 45]. The CPE is related to the surface roughness at the interface since the complex geometry leads to non-uniform charge transfer and electrical conduction. It has been shown that the fractal nature of a rough surface can be described by a power law relationship between the impedance of the surface and the frequency of the signal, which gives rise to a CPE [46, 47]. The impedance of a CPE is

$$Z_{\mathrm{CPE}}(\omega) = \frac{1}{Q(\mathrm{i}\omega)^n} \tag{1}$$

where Q is the magnitude of the CPE, n is a measure of the roughness or polarizability and has a range of (0, 1), and $\omega = 2\pi f$ is the angular frequency [45]. It can be seen that when $n = 0$, the CPE is purely resistive, and when $n = 1$, the CPE is purely capacitive. Because of the composite nature of the AgPDMS electrodes, the CPE may be a more accurate representation of the EDL, as shown in figure 3(b). Thus, it was required in our work to determine whether the ideal capacitor model or the CPE model more accurately represents the EDL.

When a cell is present between the electrodes, it contributes impedance in parallel with the channel as two capacitors C_{mem} (membrane capacitance) in series with a resistor R_{cyto} (cytoplasm resistance), as shown in figure 3(c) which assumes a CPE model for the EDL. The impedance of the system is

$$Z(\omega) = \frac{V_{\mathrm{in}}}{V_{\mathrm{out}}} G \tag{2}$$

where V_{in} is the excitation voltage, V_{out} is the output of the pre-amplifier, and G is the gain of the pre-amplifier. In experiments, impedance data was first gathered without a cell in the channel to fit to the appropriate model for device characterization (R_{ch} and C_{ch}). Impedance data was then gathered as cells flowed through the channel, which was fitted to its respective model for cell characterization (R_{cyto} and C_{mem}).

From these quantities and using Maxwell's mixture equation, the cytoplasm conductivity and specific membrane capacitance are

$$\sigma_{\mathrm{cyto}} = \frac{4\sigma_{\mathrm{m}}}{9\phi h\kappa\sigma_{\mathrm{m}} R_{\mathrm{cyto}} - 2} \tag{3}$$

$$C_{\mathrm{sp.mem}} = \frac{4}{9\phi r h\kappa} C_{\mathrm{mem}} \tag{4}$$

where $\sigma_{\mathrm{m}} = 1.6$ S m^{-1} is the conductivity of the medium (PBS), $\phi = \frac{\frac{4}{3}\pi r^3}{lwh}$ is the volume fraction (the ratio of the volume of the cell to the volume of the electrode measurement region), r is the radius of the cell, $l = 100$ μm is the length of the electrode along the channel (parallel to the direction of flow), $w = 100$ μm is the width of the channel, $h = 50$ μm is the height of the electrode and channel, and κ is a geometric factor that takes into account non-uniform aspects of the electric field such as the fringe effect [29, 30]. Low frequency (11 kHz) impedance data collected from 10 μm polystyrene beads (Sigma-Aldrich, Germany) were used for size calibration, avoiding the need for high-speed imaging since the beads are well controlled by the manufacturer in size and shape (10.0 ± 0.2 μm).

4. Results and discussion

4.1. AgPDMS characterization

Fabricating AgPDMS electrodes required the determination of adequate Ag concentrations. AgPDMS has previously been reported to be conductive at 21 vol% (or 69 wt%) for pressure sensor applications and 83 wt% for droplet detection [4, 5, 19]. In our work, we found that AgPDMS is non-conductive at 69 wt% and has excellent conductivity at 85 wt%. SEM images were taken to observe the Ag concentration on the microchannel sidewalls as well as surface roughness. Figures 4(a) and (b) show 69 wt% Ag and 85 wt% Ag concentrations, respectively. These images were taken using the backscattered electrons (BSE) imaging mode, which show the material composition of the bottom of the device and the sidewall of the channel. Since heavier elements provide a higher intensity signal, the bright dots represent Ag particles, and the remaining grey structure represents the carbon-dominant PDMS. The density of Ag is significantly higher in figure 4(b), which resulted in a much higher conductivity of the AgPDMS electrode. Figure 4(c) was taken in the standard SEM imaging mode, showing the texture of the bottom of the device and the sidewall of the channel. The clearly visible surface roughness was caused by Ag particles suggesting the modeling of the EDL as a CPE, rather than an ideal capacitor to be more appropriate. Figure 4(d) is a top–down view of the device, showing the overall uniformity of the AgPDMS electrodes.

Thin strips of AgPDMS of various Ag concentrations were fabricated with the same dimensions of the electrodes used in the microfluidic device (3 mm long, 100 μm wide, 50 μm high) to further optimize conductivity. The conductivity values at different Ag concentrations are summarized in figure 5. While concentrations greater than 81 wt% were found to have good conductivity ($>10^3$ S m^{-1}), 85 wt% was found to have much higher conductivity while having the same ease of fabrication. AgPDMS with 87 wt% Ag started to become difficult to mix and have a clumpy, flaky texture, compared to the more paste-like composition at lower concentrations. Therefore, our AgPDMS electrodes were fabricated using 85 wt% Ag.

4.2. Device characterization

Impedance spectroscopy was first performed on the microfluidic device before cells were introduced in order to determine the device's electrical parameters and if the CPE model was a more accurate representation of the EDL compared to an ideal capacitor. A frequency sweep of 109 points from 1 kHz to 6 MHz was used to determine the impedance profile of the channel. This profile was then fitted to the channel equivalent circuit model using nonlinear least squares curve fitting (MATLAB, Mathworks Inc., USA). One sample sweep is shown in figure 6, along with the fits using the CPE model and the ideal capacitor model in (a) and (b), respectively. The model using the CPE was found to have a much better fit where

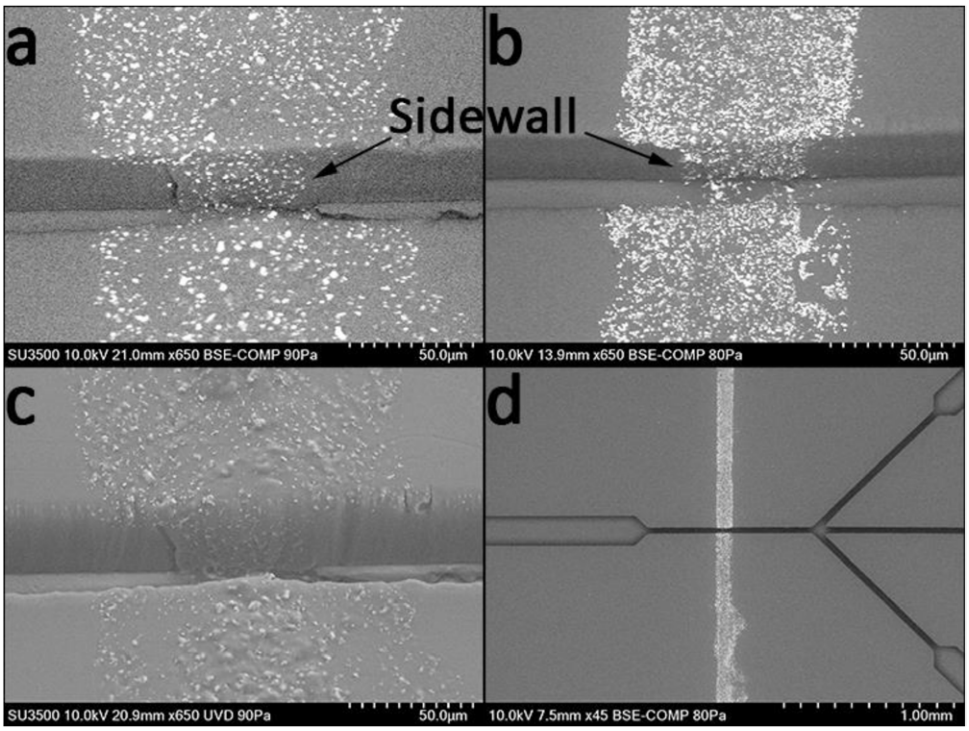

Figure 4. SEM images showing AgPDMS electrodes. (a) Device bottom and sidewall with 69 wt% Ag particles. (b) Device bottom and sidewall with 85 wt% Ag particles. (c) Surface roughness of bottom and sidewall with 85 wt% Ag particles. (d) Top–down view of device.

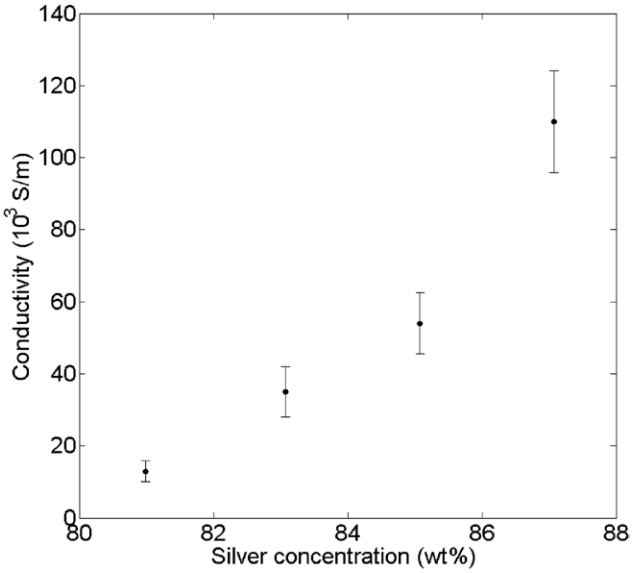

Figure 5. Conductivity of AgPDMS with varying Ag particle wt%. $n = 3$ for each Ag concentration.

the average residual error at every frequency point was on the order of 10^2, compared to the model using an ideal capacitor which had an average residual error on the order of 10^3.

The CPE model was used to represent the EDL, and eight frequency sweeps were conducted to characterize the device. The channel was found to have a resistance $R_{Ch} = 23.7 \pm 1.9\,k\Omega$ and a capacitance $C_{Ch} = 2.29 \pm 0.18$ pF. The magnitude of the CPE was found to be $Q = 1.6 \pm 0.2\ \mu S$ with exponent $n = 0.380 \pm 0.007$. In comparison, pure metal electrodes have a EDL with capacitances on the order of tens of pF [30, 34]. The CPE therefore exhibited characteristics closer to a resistive impedance than a capacitive impedance due to the inhomogeneous nature of the AgPDMS composite, and does not have as dominant an effect on the low frequency impedance data. Device characterization was performed over three days on the same device to investigate re-usability and possible contamination from experiments. The low uncertainty for each electrical parameter used to characterize the device demonstrates stability in the device. The resistance and the capacitance of the channel was recalculated before each experimental run to account for deviations in the electrode properties.

4.3. Cell measurement

Magnitude impedance data was calculated from the voltage output using an impedance spectroscope (HF2IS, Zurich Instruments, Switzerland) as cells were pressure driven to flow and pass the AgPDMS electrodes. The frequencies were chosen to be between 11 kHz and 6.01 MHz. Frequencies outside of this range were found to have poor signal-to-noise due to the EDL at low frequencies and stray capacitances at high frequency. The low end 11 kHz frequency provided size information, the high end 6.01 MHz frequency was used to probe the cytoplasm of the cell, and the frequency points in between were used to measure membrane capacitance.

Cell size is important to determine since this information is needed for normalizing cytoplasm resistance R_{cyto} and membrane capacitance C_{mem} to their intrinsic size-independent quantities (i.e. cytoplasm conductivity σ_{cyto} and specific membrane capacitance $C_{sp.mem}$). Impedance data of 10 μm beads was measured at 11 kHz for size calibration. At low frequencies, the system was almost completely resistive, and the

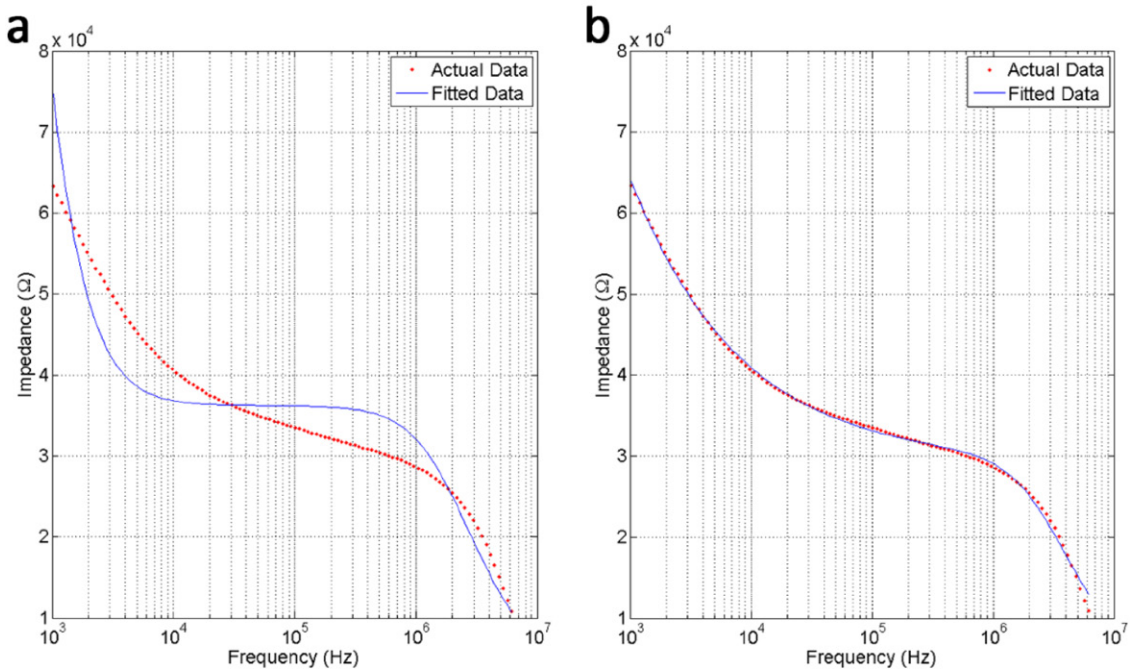

Figure 6. Impedance profile of channel without cells. (a) Data fitted with the EDL represented by an ideal capacitor. (b) Data fitted with the EDL represented by a CPE.

device behaved like a Coulter counter where the impedances of beads and cells largely depend on size and not on capacitive properties. This size data was used to differentiate large PDMS debris from cells based on size measurement in terms of signal processing.

T24 cells were used to verify the feasibility of cell detection and were detected at approximately 1 cell s^{-1}. Figure 7 shows an example segment of impedance data. Because the cell sample was not filtered before being introduced into the device, there was a wide range in peak size (figure 7) due to contaminants passing through the channel, such as PDMS debris, cell clusters, and apoptotic cells, as verified with microscopy imaging. Non-cell events, however, were easily distinguished from cell events by analyzing the impedance data. From the 2400 detected peaks, 740 cells were identified based on the size information obtained at the frequency of 11 kHz [39]. Some of the debris were determined to be over 50 μm in size (e.g. PDMS debris-caused peak as shown in figure 7). However, the 100 μm wide channel allowed passage of the debris without the occurrence of channel clogging or incurring the need for device change.

AML-2 and HL-60 cells were then tested. AML-2 and HL-60 are both human myeloid leukemia cell lines that are precursors to white blood cells [48, 49]. They both have round morphologies and are known to have similar sizes (diameters of 12.5 ± 1.3 μm versus 11.4 ± 0.93 μm for AML-2 and HL-60, respectively [28]), making them suitable models for measuring size-independent parameters. As with the T24 cells, cells were detected at 1 cell s^{-1}; and PDMS debris, cell clusters, and apoptotic cells, as determined by impedance amplitude data at 11 kHz, were removed during data analysis. From 369 detected peaks, 101 AML-2 cells were identified with a cytoplasm conductivity of 0.29 ± 0.15 S m^{-1} and a specific membrane capacitance of 41 ± 25 mF m^{-2}. From 733 detected peaks, 90 HL-60 cells were identified with a cytoplasm conductivity of 0.47 ± 0.20 S m^{-1} and a specific membrane capacitance of 55 ± 26 mF m^{-2}. As summarized in table 1, these values are on the same order of magnitude as previously reported results. The cytoplasm conductivity and

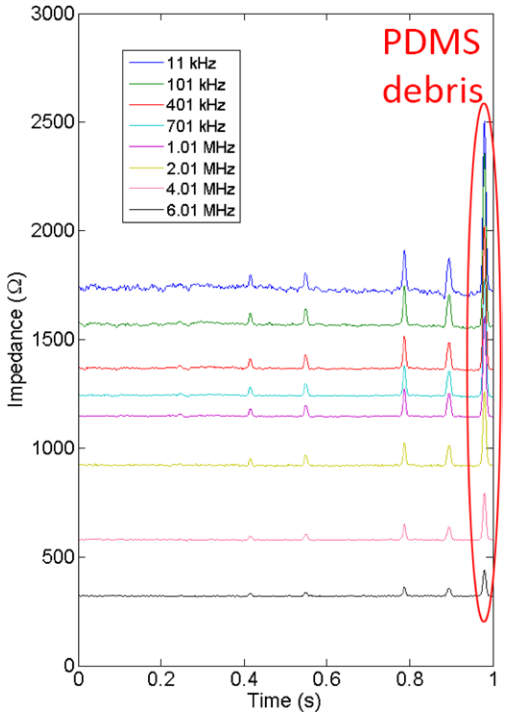

Figure 7. Eight frequency impedance data with five particles detected. Based on the data collected at 11 kHz, cell events were distinguished from non-cell events (e.g. PDMS debris and cell clusters).

Table 1. AML-2 and HL-60 electrical parameters.

Cell line		σ_{cyto} (S m^{-1})	C_{mem} (mF m^{-2})
AML-2	Measured	0.29 ± 0.15	41 ± 25
	Reference	0.62 ± 0.10	12.0 ± 1.44
HL-60	Measured	0.47 ± 0.20	55 ± 26
	Reference	0.76 ± 0.12	14.5 ± 1.75

Note: HL-60 was found to have significantly higher cytoplasm conductivity ($^*p < 0.000\,01$) and specific membrane capacitance values ($^*p < 0.0005$).

specific membrane values of HL-60 are significantly higher than those of AML-2 ($^*p < 0.000\,01$ and $^*p < 0.0005$, respectively via two-sample *t*-test) which is consistent with previous literature [28, 38]. Differences in cytoplasm conductivity and specific membrane capacitance values of AML-2 and HL-60 cells were from their different nucleus-to-cytoplasm ratios [28] and membrane morphologies [50], respectively.

Discrepancies between our measured values and previous results can be attributed to differences and limitations in the technical approaches used in this study and previous work [28]. For instance, deformed cell lengths must be determined in the constriction approach [28], based on geometrical assumptions which could have induced errors in the calculated values of cytoplasm conductivity and specific membrane capacitance. Additionally, the channel width in the constriction channel approach [28] was only 9 μm while the channel width in this work is significantly larger (100 μm). The much larger channel width in this work led to a higher noise floor in the impedance data, which further induced errors in the determined effective impedance peak caused by each cell. Furthermore, differences between our measured values and previous results can also be attributed to heterogeneity and genetic drift of cell lines resulting from passage number and slight differences in culture conditions [51]. Both AML-2 and HL-60 originate from the AML cell, which is a leukemic progenitor to leukocytes. The leukemia cell population has been shown to be highly heterogeneous, which could contribute to differences within the cell lines [52]. It has been shown that the cell cycle plays a role in regulating ion channels on the cell membrane, including potassium channels [53]. This could in turn affect the ion concentration of the cytoplasm. Cells in different cancer stages and cell lines with different differentiation grades have also been shown to have different specific membrane capacitances [39, 54]. Cell biochemistry and morphology were also found to be affected by culture time and passage number [55, 56].

In our work, single-cell peaks were properly identified, and the occurrence of device clogging was rare in experiments due to the wide channel design. PDMS was the major source of contamination in the form of debris, which occurs during unavoidable intubation procedures (filling PBS into the device, loading cells at the inlet, and attaching pressure source). Since debris complicates data analysis, implementing filtration structures [57] can help to minimize the passage of larger debris and cell clusters. The channel geometry can be further optimized as larger channels suffer from a decreased $\Delta R/R$ ratio, which could contribute to measurement error. The electrode dimensions can also be adjusted to reduce the occurrence of coincident events (multiple particles passing through the measurement region simultaneously).

5. Conclusion

This paper reported a wide channel microfluidic device that, for the first time, used integrated AgPDMS electrodes to perform single-cell electrical characterization. Compared to existing microfluidic devices for impedance spectroscopy which all use channels similar in size to that of tested cells, our device was proven by experiments to be effective in minimizing the issue of device clogging. The device is straightforward to clean and suitable for use in multiple experiments. AgPDMS sidewall electrodes were proven to limit the EDL while providing the necessary sensitivity for impedance spectroscopy measurements. Multi-frequency impedance data was fitted to equivalent circuit models to determine cytoplasm conductivity and specific membrane capacitance for each cell. Quantified values of cytoplasm conductivity (0.29 ± 0.15 S m^{-1} versus 0.47 ± 0.20 S m^{-1}) and specific membrane capacitance for AML-2 and HL-60 cells (41 ± 25 mF m^{-2} versus 55 ± 26 mF m^{-2}) are consistent with the results reported in the literature. Present work involves the investigation of effects of Ag particle size (nanoparticles versus microparticles) and shape (isotropic versus anisotropic) on conductivity and EDL.

References

[1] McDonald J C and Whitesides G M 2002 Poly(dimethylsiloxane) as a material for fabricating microfluidic devices *Acc. Chem. Res.* **35** 491–9
[2] Holmes D, She J K, Roach P L and Morgan H 2007 Bead-based immunoassays using a micro-chip flow cytometer *Lab Chip* **7** 1048–56
[3] Bhagat A A S, Jothimuthu P and Papautsky I 2007 Photodefinable polydimethylsiloxane (PDMS) for rapid lab-on-a-chip prototyping *Lab Chip* **7** 1192–7
[4] Niu X Z, Peng S L, Liu L Y, Wen W J and Sheng P 2007 Characterizing and patterning of PDMS-based conducting composites *Adv. Mater.* **19** 2682–6
[5] Cong H and Pan T 2008 Photopatternable conductive PDMS materials for microfabrication *Adv. Funct. Mater.* **18** 1912–21
[6] Wang L, Zhang M, Yang M, Zhu W, Wu J, Gong X and Wen W 2009 Polydimethylsiloxane-integratable micropressure sensor for microfluidic chips *Biomicrofluidics* **3** 34105
[7] Sherman R D, Middleman L M and Jacobs S M 1983 Electron transport processes in conductor-filled polymers *Polym. Eng. Sci.* **23** 36–46
[8] Chuang H-S and Wereley S 2009 Design, fabrication and characterization of a conducting PDMS for microheaters and temperature sensors *J. Micromech. Microeng.* **19** 045010
[9] Deman A-L, Brun M, Quatresous M, Chateaux J-F, Frenea-Robin M, Haddour N, Semet V and Ferrigno R 2011 Characterization of C-PDMS electrodes for electrokinetic applications in microfluidic systems *J. Micromech. Microeng.* **21** 095013
[10] Niu X, Wen Wand Lee Y K 2005 Electrorheological-fluid-based microvalves *Appl. Phys. Lett.* **87** 1–3

[11] Liu L, Chen X, Niu X, Wen W and Sheng P 2006 Electrorheological fluid-actuated microfluidic pump *Appl. Phys. Lett.* **89** 87–90
[12] Niu X, Liu L, Wen W and Sheng P 2006 Hybrid approach to high-frequency microfluidic mixing *Phys. Rev. Lett.* **97** 3–6
[13] Wang H, Wang J, Hong J, Wei Q, Gao W and Zhu Z 2007 Preparation and characterization of silver nanocomposite textile *J. Coat. Technol. Res.* **4** 101–6
[14] Myllymaa S, Pirinen S, Myllymaa K, Suvanto M, Pakkanen T A, Pakkanen T T and Lappalainen R 2012 Improving electrochemical performance of flexible thin film electrodes with micropillar array structures *Meas. Sci. Technol.* **23** 125701
[15] Zhu L, Xie D, Ma J, Shao J and Shen X 2013 Fabrication of polydimethylsiloxane composites with nickel particles and nickel fibers and study of their magnetic properties *Smart Mater. Struct.* **22** 045015
[16] Sosa M, Bernal-Alvarado J, Jiménez-Moreno M, Hernández J C, Gutiérrez-Juárez G, Vargas-Luna M, Huerta R, Villagómez-Castro J C and Palomares P 2005 Magnetic field influence on electrical properties of human blood measured by impedance spectroscopy *Bioelectromagnetics* **26** 564–70
[17] Liu L, Peng S, Niu X and Wen W 2006 Microheaters fabricated from a conducting composite *Appl. Phys. Lett.* **89** 223521
[18] Liu L, Peng S, Wen W and Sheng P 2007 Paperlike thermochromic display *Appl. Phys. Lett.* **90** 68–71
[19] Niu X, Zhang M, Peng S, Wen W and Sheng P 2007 Real-time detection, control, and sorting of microfluidic droplets *Biomicrofluidics* **1** 44101
[20] Schwan H P 1957 Electrical properties of tissues and cell suspensions *Adv. Biol. Med. Phys.* **5** 147–209
[21] Zheng Y, Nguyen J, Wei Y and Sun Y 2013 Recent advances in microfluidic techniques for single-cell biophysical characterization *Lab Chip* **13** 2464–83
[22] Coulter W H 1956 High speed automatic blood cell counter and cell size analyzer *Proc. National Electronics Conf.* vol 12 pp 1034–40
[23] Hoffman R A and Britt W B 1979 Flow-system measurement of cell impedance properties *J. Histochem. Cytochem.* **27** 234–40
[24] Huang Y, Wang X B, Hölzel R, Becker F F and Gascoyne P R 1995 Electrorotational studies of the cytoplasmic dielectric properties of Friend murine erythroleukaemia cells *Phys. Med. Biol.* **40** 1789–806
[25] Wang X B, Huang Y, Gascoyne P R, Becker F F, Hölzel R and Pethig R 1994 Changes in Friend murine erythroleukaemia cell membranes during induced differentiation determined by electrorotation *Biochim. Biophys. Acta* **1193** 330–44
[26] Ayliffe H E, Frazier A B and Rabbitt R D 1999 Microchannels with integrated metal electrodes *IEEE J. Microelectromech. Syst.* **8** 50–7
[27] Gawad S, Schild L and Renaud P H 2001 Micromachined impedance spectroscopy flow cytometer for cell analysis and particle sizing *Lab Chip* **1** 76–82
[28] Zheng Y, Shojaei-Baghini E, Wang C and Sun Y 2013 Rapid measurement of specific membrane capacitance and cytoplasm conductivity on single cells *Proc. IEEE Int. Conf. Micro Electro Mechanical System* vol 42 pp 1105–8
[29] Gawad S, Cheung K, Seger U, Bertsch A and Renaud P 2004 Dielectric spectroscopy in a micromachined flow cytometer: theoretical and practical considerations *Lab Chip* **4** 241–51
[30] Morgan H, Sun T, Holmes D, Gawad S and Green N G 2007 Single cell dielectric spectroscopy *J. Phys. D: Appl. Phys.* **40** 61–70
[31] Holmes D, Pettigrew D, Reccius C H, Gwyer J D, van Berkel C, Holloway J, Davies D E and Morgan H 2009 Leukocyte analysis and differentiation using high speed microfluidic single cell impedance cytometry *Lab Chip* **9** 2881–9
[32] Sun T, Green N G, Gawad S and Morgan H 2007 Analytical electric field and sensitivity analysis for two microfluidic impedance cytometer designs *IET Nanobiotechnol.* **1** 69–79
[33] Han X, van Berkel C, Gwyer J, Capretto L and Morgan H 2012 Microfluidic lysis of human blood for leukocyte analysis using single cell impedance cytometry *Anal. Chem.* **84** 1070–5
[34] Gamburg Y D and Zangari G 2011 *Theory and Practice of Metal Electrodeposition* (Berlin: Springer)
[35] Zhou J, Ren K, Zheng Y, Su J, Zhao Y, Ryan D and Wu H 2010 Fabrication of a microfluidic Ag/AgCl reference electrode and its application for portable and disposable electrochemical microchips *Electrophoresis* **31** 3083–9
[36] Wang H and Lu C 2006 Electroporation of mammalian cells in a microfluidic channel with geometric variation exogenous molecules into cells. Rapid electrical lysis *Chem. Anal.* **78** 5158–64
[37] Ryu K S, Wang X, Shaikh K and Liu C 2004 A method for precision patterning of silicone elastomer and its applications *J. Microelectromech. Syst.* **13** 568–75
[38] Tan Q, Ferrier G A, Chen B K, Wang C and Sun Y 2012 Quantification of the specific membrane capacitance of single cells using a microfluidic device and impedance spectroscopy measurement *Biomicrofluidics* **6** 34112
[39] Liu H, Tan Q, Geddie W R, Jewett M A S, Phillips N, Ke D, Simmons C A and Sun Y 2014 Biophysical characterization of bladder cancer cells with different metastatic potential *Cell Biochem. Biophys.* **68** 241–6
[40] Zheng Y, Shojaei-Baghini E, Azad A, Wang C and Sun Y 2012 High-throughput biophysical measurement of human red blood cells *Lab Chip* **12** 2560–7
[41] Zheng Y, Nguyen J, Wang C and Sun Y 2013 Electrical measurement of red blood cell deformability on a microfluidic device *Lab Chip* **13** 3275–83
[42] Maxwell J C 1954 *A Treatise on Electricity and Magnetism* vol 1 (New York: Dover)
[43] Sun T, Holmes D, Gawad S, Green N G and Morgan H 2007 High speed multi-frequency impedance analysis of single particles in a microfluidic cytometer using maximum length sequences *Lab Chip* **7** 1034–40
[44] Brug G J, van den Eeden A L G, Sluyters-Rehbach M and Sluyters J H 1984 The analysis of electrode impedances complicated by the presence of a constant phase element *J. Electroanal. Chem. Interfacial Electrochem.* **176** 275–95
[45] Bates J B, Chu Y T and Stribling W T 1988 Surface topography and impedance of metal-electrolyte interfaces *Phys. Rev. Lett.* **60** 627–30
[46] Koch D L 1991 The AC electrical impedance of a fractal boundary to an electrolytic solution *J. Electrochem. Soc.* **138** 475
[47] Wang Y-B, Yuan R-K and Willander M 1996 Capacitance of semiconductor-electrolyte junction and its frequency dependence *Appl. Phys.* A **63** 481–6
[48] Tiacci E, Spanhol-Rosseto A, Martelli M P, Pasqualucci L, Quentmeier H, Grossmann V, Drexler H G and Falini B 2012 The NPM1 wild-type OCI-AML2 and the NPM1-mutated OCI-AML3 cell lines carry DNMT3A mutations *Leukemia* **26** 554–7
[49] Gallagher R *et al* 1979 Characterization of the continuous, differentiating myeloid cell line (HL-60) from a patient with acute promyelocytic leukemia *Blood* **54** 713–33
[50] Gamliel H, Gurfel D and Polliack A 1983 Utilization of monoclonal antibodies and immuno-scanning electron microscopy for the positive identification of human leukemic cells *J. Clin. Immunol.* **3** 399–407
[51] Hughes P, Marshall D, Reid Y, Parkes H and Gelber C 2007 The costs of using unauthenticated, over-passaged cell

lines: how much more data do we need? *Biotechniques* **43** 575–86
[52] McCulloch E A 1993 Stem cell renewal and determination during clonal expansion in normal and leukaemic haemopoiesis *Cell Prolif.* **26** 399–425
[53] Urrego D, Tomczak A P, Zahed F, Stühmer W and Pardo L A 2014 Potassium channels in cell cycle and cell proliferation *Phil. Trans. R. Soc.* B **369** 20130094
[54] Salmanzadeh A, Sano M B, Gallo-Villanueva R C, Roberts P C, Schmelz E M and Davalos R V 2013 Investigating dielectric properties of different stages of syngeneic murine ovarian cancer cells *Biomicrofluidics* **7** 1–12
[55] Briske-Anderson M J, Finley J W and Newman S M 1997 The influence of culture time and passage number on the morphological and physiological development of Caco-2 cells *Proc. Soc. Exp. Biol. Med.* **214** 248–57
[56] Volpe D A 2008 Variability in Caco-2 and MDCK cell-based intestinal permeability assays *J. Pharm. Sci.* **97** 712–25
[57] Nguyen J, Wei Y, Zheng Y, Wang C and Sun Y 2015 On-chip sample preparation for complete blood count from raw blood *Lab Chip* **15** 1533–44